Exchange bias and enhancement of the Néel temperature in thin NiF_2 films

Hongtao Shi and D. Lederman
Department of Physics, West Virginia University, Morgantown, West Virginia 26506-6315, USA

K. V. O'Donovan*
Department of Materials Science and Engineering, University of Maryland, College Park, Maryland 20742-2115, USA and National Institute of Standards and Technology, Gaithersburg, Maryland 20899, USA

J. A. Borchers
National Institute of Standards and Technology, Gaithersburg, Maryland 20899, USA
(Received 29 December 2003; revised manuscript received 25 March 2004; published 21 June 2004)

Epitaxial thin (110) films of the weak ferromagnet NiF_2 were deposited on single-crystal MgF_2 (110) substrates via molecular-beam epitaxy. Subsequently polycrystalline Co was grown on the NiF_2 film. The antiferromagnetic ordering of the NiF_2 was monitored as a function of temperature via neutron diffraction and the exchange bias H_E of the Co layers was measured via standard magnetometry measurements. Because in NiF_2 the spins lie in the (001) plane, the maximum H_E is observed after cooling the sample with a cooling field in the film plane perpendicular to the [001] direction of the NiF_2. In 60 nm, 49 nm, and 38 nm thick NiF_2 samples, the Néel temperature is $T_N \approx 81$ K, which is significantly larger than the bulk value of $T_N = 73.2$ K. This enhancement also occurs in films without Co overlayers and thus is not due to a proximity effect. For the 38 nm sample with a Co overlayer cooled in a 50 kOe field, $H_E > 0$ and vanishes at a blocking temperature (T_B) which coincides with the T_N of the films. When the sample is cooled in 2.0 kOe, $H_E < 0$, disappearing at $T = 55$ K, reappearing at $T = 65$ K, and finally disappearing once again at $T = 81$ K. For the 12 nm thick NiF_2 sample, $T_B \ll T_N$. Strain-induced enhancement of ferromagnetic exchange interactions between the nearest-neighbor Ni^{2+} ions along the c axis may be responsible for the T_N enhancement. These results also demonstrate that in general, a diminished T_B is not necessarily due to a lower T_N.

DOI: 10.1103/PhysRevB.69.214416 PACS number(s): 75.70.Cn, 75.25.+z, 75.30.Gw, 75.50.Ee

I. INTRODUCTION

Exchange bias (H_E) refers to the shift of the magnetic hysteresis loop of a ferromagnet (F) away from $H = 0$ when the F is coupled to an antiferromagnet (AF) or a ferrimagnet. It was originally discovered in Co particles whose surface was oxidized to form CoO.[1] This effect has been observed in a large number of systems, including ferrimagnetic/ferromagnetic bilayers.[2,3] H_E vanishes above a temperature conventionally denoted as the blocking temperature T_B. Bilayer systems in which the AF is below a critical thickness t_C, which is system dependent, generally have a much lower T_B compared to the Néel ordering temperature T_N of the bulk AF.[4,5] This reduction of T_B could be due to the decrease of T_N because of finite size or strain effects,[6,7] but it is often difficult to unambiguously distinguish between T_B and T_N. By performing neutron diffraction on single crystalline Fe_3O_4/CoO multilayers, it was recently shown that the T_N of CoO layers increases when the thickness of CoO is less than 5 nm, whereas T_B decreases in that thickness regime.[8] This increase in T_N was interpreted to arise from the proximity of the CoO layers to the ferrimagnetic Fe_3O_4 layers, which have a much higher-ordering temperature than CoO (for bulk Fe_3O_4 $T_C = 858$ K, and for bulk CoO $T_N = 291$ K). It was also recently reported that the FeF_2 thin film T_N can be enhanced to $T_N \sim 82$ K (bulk $T_N = 78.4$ K) when FeF_2/ZnF_2 multilayers are grown on MgO (100) substrates with FeF_2 layer thicknesses between 10 and 15 monolayers.[9] This enhancement was attributed to the strain in FeF_2 due to the small lattice mismatch between these two materials.

In this paper we report on the epitaxial growth and exchange bias of the weak ferromagnet NiF_2. We find several interesting new phenomena, including: (1) a significant increase in T_N with respect to bulk, possibly due to strain; (2) a significant exchange bias in NiF_2 films with Co overlayers; (3) a reentrant exchange bias behavior for intermediate (38 nm) NiF_2 thin-film thicknesses; and (4) a significant difference in the T_N and T_B for thin NiF_2 samples (12 nm). These results are discussed in terms of the known magnetic properties of NiF_2.

The properties of NiF_2 in bulk form can be summarized as follows. NiF_2 shares the rutile crystal structure with MgF_2, FeF_2, MnF_2, CoF_2, and ZnF_2, having lattice constants $a = b = 0.4651$ nm and $c = 0.3084$ nm at room temperature.[10] For NiF_2 the magnetic Hamiltonian is[11]

$$\mathcal{H} = -\sum_{i,j,i\neq j} J_{ij}\vec{S}_i \cdot \vec{S}_j + A\sum_i S_{iz}^2 + E\left[\sum_i (S_{ix'}^2 - S_{iy'}^2) - \sum_j (S_{jx'}^2 - S_{jy'}^2)\right], \quad (1)$$

where J_{ij} are magnetic exchange interactions between Ni^{2+} ions, A is a single-ion magnetic anisotropy, E is an additional anisotropy term arising from spin-orbit coupling in the Ni^{2+} ions, and the x' and y' axes are at 45° relative to the crystalline a and b axes. Also in the third term, the sums over spins i and j refer to spins on opposite sublattices. Because the single-ion anisotropy term A is positive, at low tempera-

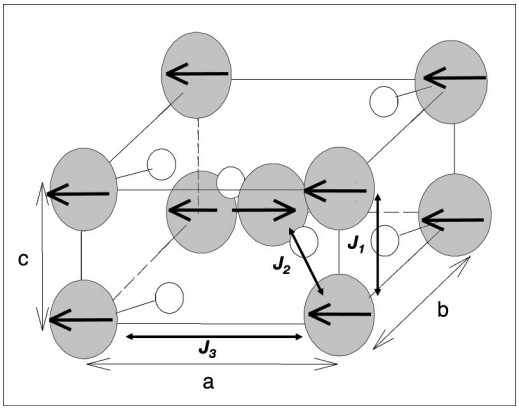

FIG. 1. Crystalline NiF_2 structure (small and large circles represent F^- and Ni^{2+} ions, respectively) with one possible magnetic arrangement at low temperatures. Another possible arrangement is with the spins along the *b* axis. The exchange interactions J_1, J_2, and J_3 are indicated.

tures the spins lie in the (001) plane, in contrast to FeF_2, MnF_2, and CoF_2, where $A<0$ (resulting in spins along the [001] direction). The competition between the rhombic term E (in the other fluorides ~ 0), which tends to align the spins perpendicular to each other, and the exchange term, which tends to align them antiparallel to each other, causes a canting of the spins in the *a*-*b* plane.[12] Because $E \ll Jz$, with $z=8$ being the number of next-nearest neighbors for each site, the canting angle is small, approximately 0.43°.[12] This results in a small spontaneous magnetic moment, and hence NiF_2 is a weak ferromagnet. Single-crystal samples in principle can be made into a single magnetic domain by applying a large field along the [100] or [010] direction below T_N.[13] The value of $T_N=73.2$ K has been verified on bulk single crystals via heat capacity,[13] magnetization,[14] and thermal expansion[15] measurements. The low-temperature magnetic structure and the dominant exchange interactions are shown in Fig. 1.

The exchange constants have been determined from inelastic neutron scattering:[12] $J_1=0.22$ cm^{-1} (ferromagnetic coupling between ions along the *c* axis, nearest neighbors), $J_2=-13.87$ cm^{-1} (antiferromagnetic coupling between corner to body center ions, next-nearest neighbors), $J_3=-0.79$ cm^{-1} (antiferromagnetic coupling between ions along the *a* or *b* axis, next-next-nearest neighbors). Note that $J_2 \gg J_1, J_3$, and thus dominates the exchange interactions. Spins in (110) planes are almost compensated, except for the small spontaneous canting, since the magnetic moments of the Ni^{2+} ions on the vertices of the body-centered tetragonal (bct) lattice tend to point opposite to those at the center of the unit cell.

II. EXPERIMENTAL DETAILS

A. Growth

All samples were grown on commercially grown and polished (110) MgF_2 single-crystal substrates by molecular-beam epitaxy (MBE) at a growth rate of ~ 0.02 nm/s, monitored by quartz-crystal monitors. The substrate was rinsed in methanol for 10 min prior to transfer to the MBE chamber with a base pressure of 1.0×10^{-9} mbar. Before the deposition, the substrate was heated to 297 °C for 30 min. NiF_2 was then deposited onto the substrate by electron-beam evaporation of compressed NiF_2 pellets. The growth pressure during evaporation was $\sim 5.0\times10^{-8}$ mbar. After the growth of the NiF_2 layer, a polycrystalline Co film, with a nominal thickness of 18 nm, was deposited at 125 °C. The actual thicknesses were measured after growth via x-ray reflectivity, as discussed below. In order to prevent oxidation, all samples were capped with 5 nm MgF_2 deposited at room temperature.

B. Structural characterization

The surface crystal structure was analyzed *in situ* via reflection high-energy electron diffraction (RHEED). The crystallography and interface structure was analyzed *ex situ* from x-ray diffraction and reflectivity data, obtained from a rotating anode source using Cu $K\alpha$ radiation. In-plane lattice parameters were determined from Bragg reflections with a component of the x-ray momentum-transfer vector q pointing in the plane of the sample.[16,17] Reflectivity data were fit to a recursive optical model to determine the thickness of each layer, as well as the interface roughness between adjacent layers.[18]

C. Magnetization measurements

The exchange bias was measured in a superconducting quantum interference device (SQUID) magnetometer after field cooling the sample from $T=100$ K to $T=5$ K. Both the cooling field H_{CF} and the measuring field H were applied parallel to the NiF_2 [110] direction, that is, in the plane of the sample and perpendicular to the *c* axis. No exchange bias was observed if H_{CF} was applied parallel to the *c* axis. This may occur because the moments in the F and AF layers are perpendicular to each other during cooling in this situation, so that the net interface interaction between the antiferromagnet and the ferromagnet is $J_I \vec{S}_F \cdot \vec{S}_{AF}=0$, where J_I is an effective interface exchange interaction and $\vec{S}_F$ and $\vec{S}_{AF}$ are the spins in the F and AF layers, respectively.[19]

Additional measurements were carried out using a vibrating sample magnetometer (VSM) which allowed us to cool the sample in a magnetic field and then rotate the sample at low temperatures in order to measure $M \perp H_{CF}$.

D. Magnetic neutron diffraction

Neutron-diffraction measurements were carried out at the NIST Center for Neutron Research. The BT-2 and BT-9 triple-axis spectrometers were used with a neutron wavelength of 0.235 nm. A closed cycle refrigerator was used to cool the sample to 12 K. The (001)NiF_2 magnetic Bragg reflection, which is sensitive to the ordering of spins in the (001) planes, was monitored as a function of temperature in order to determine T_N. Note that the existence of this reflection also proves that the magnetic order in the film is that of NiF_2. This peak is normally absent for the other antiferromagnetic rutile fluorides (FeF_2, MnF_2, and CoF_2) due to the

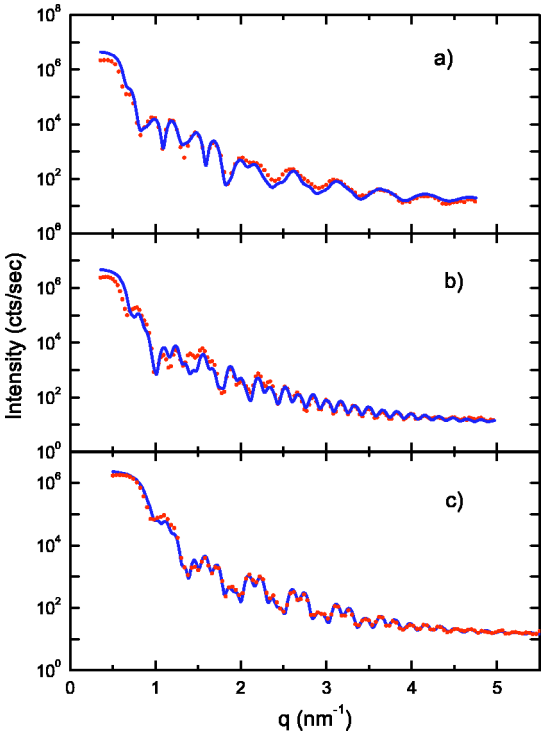

FIG. 2. Specular x-ray reflectivity intensity as a function of the x-ray wave vector $\vec{q}$ for NiF_2/Co bilayers with NiF_2 thicknesses of (a) 12 nm, (b) 38 nm, and (c) 49 nm. The dots are the acquired data and the solid lines are fits to a fully optical reflectivity model. The interface roughness parameters resulting from the fit are shown in Table I. For (a) and (b) the fitted intensity below the critical edge is larger than the measured data because at those angles that size of the sample was smaller than the x-ray beam footprint.

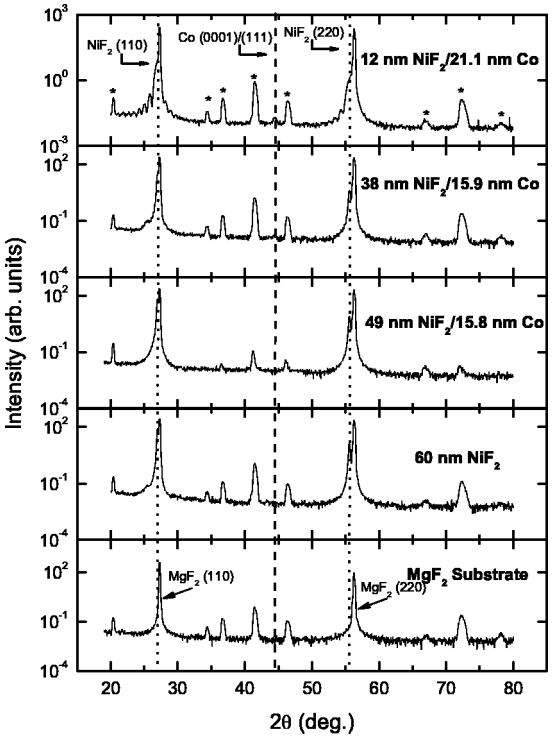

FIG. 3. θ-2θ x-ray diffraction scans of the samples used in this study. The observed NiF_2 reflections are indicated by the dotted vertical lines. The dashed vertical line is the position of the Co fcc (111) or hcp (0001) reflection. The bottom panel is a scan of the substrate without overlayers, and the MgF_2 (110) and (220) peaks are labeled. The other peaks in the bottom panel, labeled with a (*) on the top panel, are unidentified substrate impurities.

neutron magnetic scattering selection rules for their localized spins pointing along the [001] direction.[20]

III. RESULTS AND DISCUSSION

A. Structure

Given that epitaxial growth of NiF_2 films has not, to the best of our knowledge, been reported previously, we present a detailed description of the structure of our films.

Figure 2 shows x-ray reflectivity scans for three NiF_2/Co bilayers. The fit parameters are summarized in Table I. The fits show that the roughness at the NiF_2/Co interface is $\approx$0.3 nm, which is significantly smaller than the roughness observed in single-crystal FeF_2/Co bilayers ($\sigma \approx 0.8$ nm).[21] On the other hand, the Co surface is much rougher than the NiF_2 surface (see Table I), as is the case in FeF_2/Co bilayers.

Figure 3 shows the out-of-plane x-ray diffraction scan for the samples used in this study. The films are clearly strongly (110) oriented. For the two thinnest samples, finite-size fringes can be observed about the (110) and (220) reflections, indicating that the top and bottom surfaces of the NiF_2 films are very smooth, in qualitative agreement with the reflectivity data. For the two thinnest samples, a Co hcp (0001) or fcc (111) peak is also observed. A Lorentzian rocking curve was observed for the NiF_2 (220) reflection with a full width at half maximum (FWHM) of 0.19°, which is significantly smaller than widths of FeF_2 films of similar thickness grown on MgO (100) (twinned with FWHM=1.8°) and on MgF_2 (110) (single crystalline with FWHM=0.50°). This is illustrated in Fig. 4.

TABLE I. Structural parameters obtained from the x-ray reflectivity shown in Fig. 2. t are the thicknesses and σ are the interface roughness parameters. All values in nanometers. Uncertainties for t are $\approx \pm 0.2$ nm and $\approx \pm 0.2$ nm for σ.

NiF_2 t	Co t	MgF_2	σ NiF_2/subst	σ Co/NiF_2	σ MgF_2/Co	σ air/MgF_2
12.0	21.1	5.0	0.3	0.2	1.9	1.0
38.0	15.9	5.0	0.4	0.3	1.2	0.8
49.0	15.8	5.0	0.3	0.3	1.0	1.0

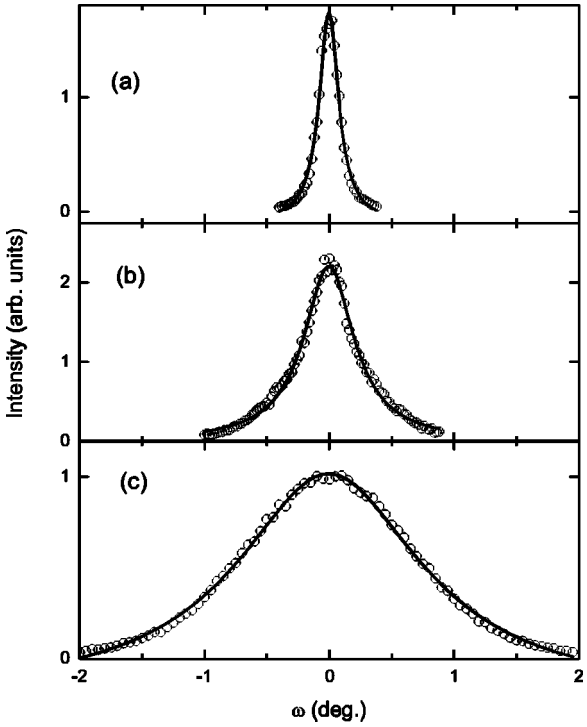

FIG. 4. Rocking curves for the (220) peaks of (a) 60 nm NiF_2 grown on MgF_2 (110); (b) 68 nm FeF_2 grown on MgF_2 (110); and (c) 69 nm FeF_2 grown on MgO (100). All samples were grown under similar conditions. Samples grown on MgF_2 are epitaxial single crystalline while the sample grown on MgO (100) is twinned with two equivalent in-plane *c* axes. The circles are the data and the solid curves are fits to Lorentzian line shapes. The widths of the fits are 0.19°, 0.50°, and 1.8°, respectively.

X-ray diffraction ϕ scans demonstrated that the NiF_2 grows epitaxially on the MgF_2. Figures 5(a) and 5(b) show the in-plane ϕ scans of the 60 nm thick single NiF_2 film and its substrate. The scans were carried out with the incident beam and the detector fixed at the NiF_2 (332) and MgF_2 (332) Bragg conditions while the sample was rotated about

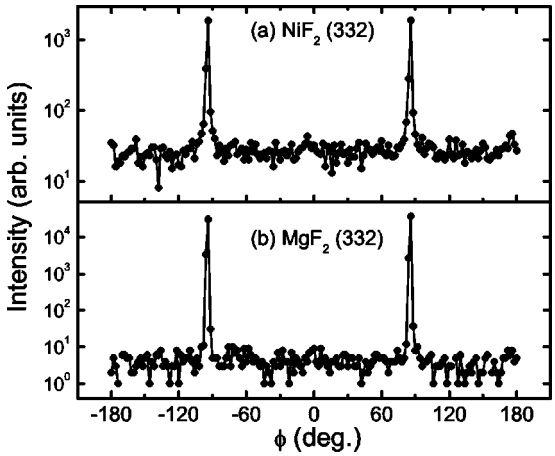

FIG. 5. Typical ϕ scans for the (a) NiF_2 (332) and (b) MgF_2 (332) Bragg reflections used to determine the epitaxial relationship of NiF_2 to the substrate: NiF_2 [001] ∥ MgF_2 [001] and NiF_2 [110] ∥ MgF_2 [110]. Lines are guides to the eye.

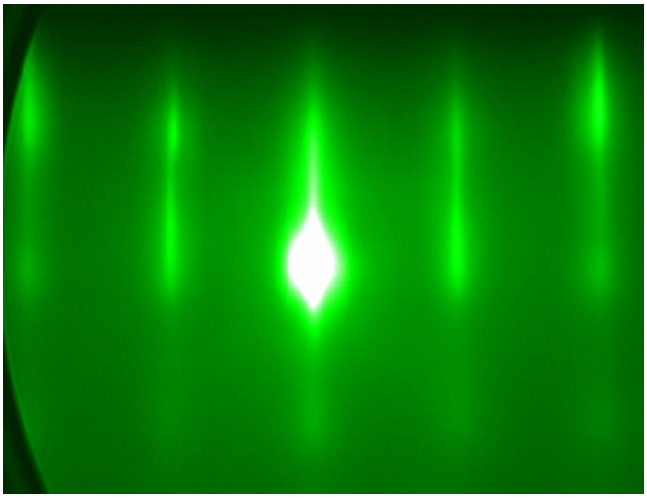

FIG. 6. RHEED pattern of the 60 nm NiF_2 sample with the electron beam incident parallel to NiF_2 [110] direction.

the surface normal. Combining the out-of-plane and in-plane scans, the epitaxial relationship was determined to be NiF_2 [001] ∥ MgF_2 [001] and NiF_2 [110] ∥ MgF_2 [110]. This was confirmed by RHEED patterns obtained after the NiF_2 layer growth, as shown in Fig. 6. This pattern, obtained with the incident beam along the NiF_2 [110] direction for the 60 nm thick sample, was only twofold symmetric as a result of the twofold symmetry of the (110) surface. Furthermore, the streaky nature of the pattern qualitatively indicates that the surface is crystalline and smooth. The in-plane lattice parameters were determined from Bragg reflections with a component of $\vec{q}$ being parallel and perpendicular to the in-plane [001] direction. Figure 7 shows θ-2θ scans of the NiF_2 (332) and (420) Bragg reflections, as well as the fittings to Gaussian line shapes. After transforming the base vectors from bct $a=[100]$, $b=[010]$, and $c=[001]$ to $a'=[110]$, $b'=[110]$, and

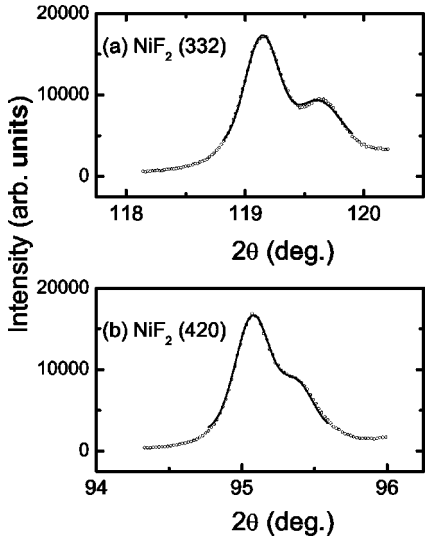

FIG. 7. θ-2θ scans of the (332) and (420) peaks of a 60 nm NiF_2 sample. The two peaks correspond to the Cu $K_{\alpha 1}$ and Cu $K_{\alpha 2}$ wavelengths. The data are the dots and the curves are fits to two Gaussians.

TABLE II. Lattice constants d_{hkl} for NiF_2. Bulk NiF_2 and MgF_2 values obtained from Refs. 10 and 22, respectively. NiF_2 thin-film values obtained from this work. The 60 nm sample does not have a Co overlayer. Values in nanometers. Uncertainties for thin-film lattice parameters are ±0.0002 nm.

Sample	d_{110}	d_{110}	d_{001}
Bulk MgF_2	0.3267	0.3267	0.3040
Bulk NiF_2	0.3289	0.3289	0.3084
60 nm NiF_2	0.3307	0.3272	0.3056
49 nm NiF_2	0.3304		0.3058
38 nm NiF_2	0.3304		0.3061
12 nm NiF_2	0.3302		0.3061

$c'=[001]$, we see that the (332) and (420) reflections in the bct coordinate system become (302) and (310) reflections in the new indexing system. Because the [110] direction is the growth direction, and the a' lattice parameter is known from the out-of-plane scan, c' and b' can be easily calculated. Results are shown in Table II, along with the lattice constant of bulk NiF_2 and MgF_2 and the [110] and [001] lattice parameters for the other samples used in this study. From the table it is clear that the NiF_2 contracts along [001] and [110] directions due to the smaller lattice constant of the MgF_2 substrate. However, along the surface normal, such restriction does not exist, leading to a lattice expansion along that direction. Although d_{110} was not directly measured for the thinner films, it is safe to assume that it is similar to the 60 nm film value because of the similar d_{001} values. Note that within the uncertainty of our measurements there is very little variation of the lattice parameters as a function of NiF_2 thickness, indicating that the strain is similar in all of our thin-film samples. The width of diffraction peaks with $\vec{q}$ perpendicular to the surface and partially in the plane[17] indicated that the out-of-plane and in-plane coherence lengths for the 60 nm film were 35.7 nm and 29.4 nm, respectively.

B. General magnetic properties of the samples

Representative magnetization hysteresis loops for the 49 nm sample are shown in Fig. 8. Figures 9–11 show how the exchange bias, coercivity (H_C), and neutron magnetic peak intensity depend on temperature for the 49 nm, 38 nm, and 12 nm samples, respectively. In all the magnetization measurements $H_{CF}=2$ kOe was applied parallel to the NiF_2 [110] direction. Note that for the two thicker samples H_C has a peak that does *not* coincide with T_B, unlike what is observed in single crystal FeF_2/Co and twinned FeF_2/Fe samples, where the position of the peak coincides with T_B.[23–25] The origin of this peak in FeF_2 has been attributed to short-range order above T_N,[25] to the properties of the surface antiferromagnetic susceptibility,[23] or to uncompensated spins due to domain formation in the antiferromagnet.[26] A similar mechanism may be responsible for the behavior in NiF_2. Also note that for the 49 nm sample $H_E>0$, which also occurs for FeF_2 cooled in high fields.[27] We have verified that $H_E<0$ at $T=5$ K when cooling in $H_{CF}=1$ kOe. These issues will be studied in more detail in a future publication.

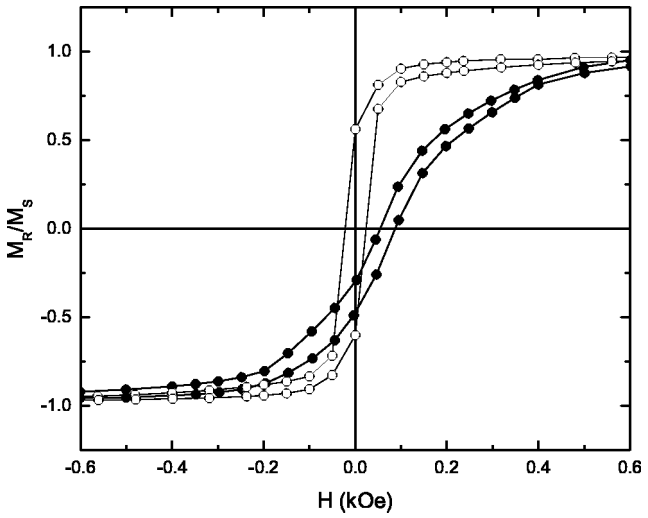

FIG. 8. Magnetization hysteresis loops for the 49 nm NiF_2/15.8 nm Co bilayer sample. Data obtained at $T=90$ K (○) and $T=5$ K (•), the latter after field cooling in $H_{CF}=2$ kOe. H and H_{CF} were applied along the NiF_2 [110] direction.

C. Enhancement of the NiF_2 Néel temperature

Table III summarizes T_N and T_B for the different samples. Except for the thinnest sample, T_B, $T_N\approx 81$ K, a significant

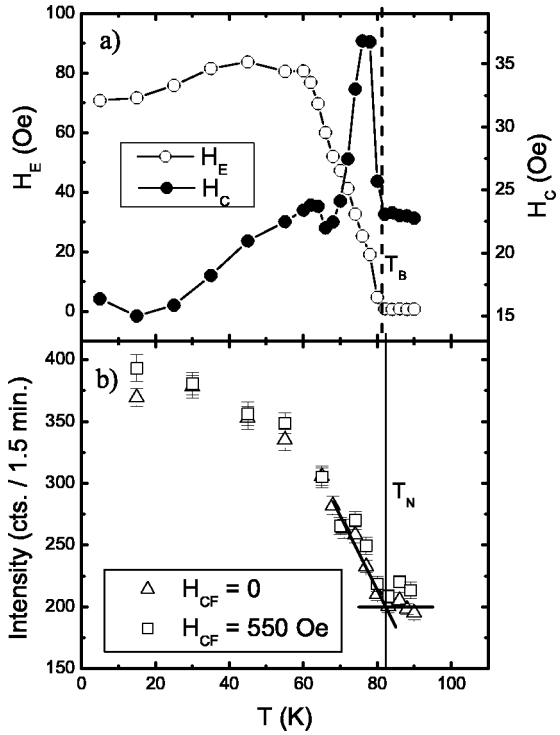

FIG. 9. (a) Exchange bias and coercive field of a 49 nm NiF_2/15.8 nm Co bilayer as a function of temperature after cooling in $H_{CF}=2$ kOe. (b) Temperature dependence of the (001) NiF_2 neutron magnetic peak intensity after field cooling in $H_{CF}=550$ Oe and $H_{CF}=0$. Solid lines are linear fits to the data points close to T_N for $H_{CF}=0$. The intersection of the lines yields T_N. The dashed vertical line indicates T_B and the solid vertical line indicates T_N.

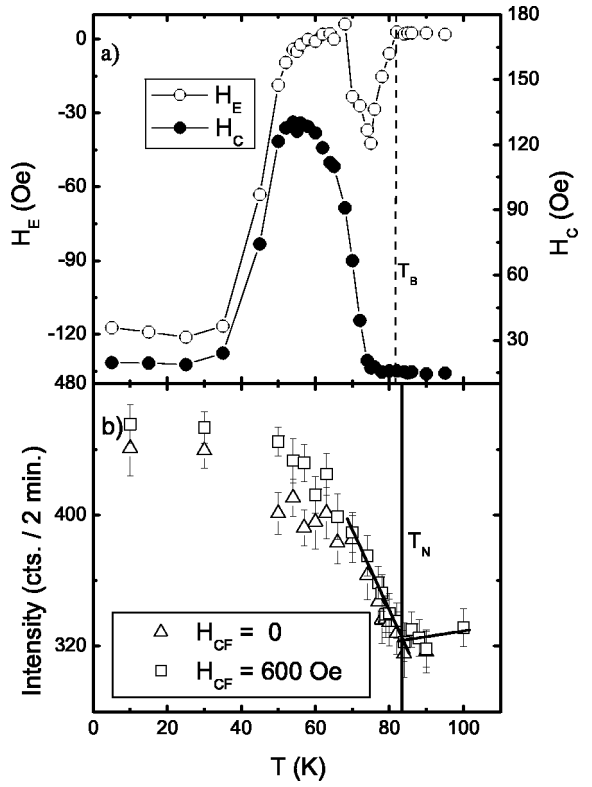

FIG. 10. (a) Exchange bias and coercive field of a 38 nm NiF_2/15.9 nm Co bilayer as a function of temperature after cooling in $H_{CF}=2$ kOe. (b) Temperature dependence of the (001) NiF_2 neutron magnetic peak intensity after field cooling in $H_{CF}=600$ Oe and $H_{CF}=0$. Solid lines are linear fits to the data points close to T_N for $H_{CF}=0$. The intersection of the lines yields T_N. The dashed vertical line indicates T_B and the solid vertical line indicates T_N.

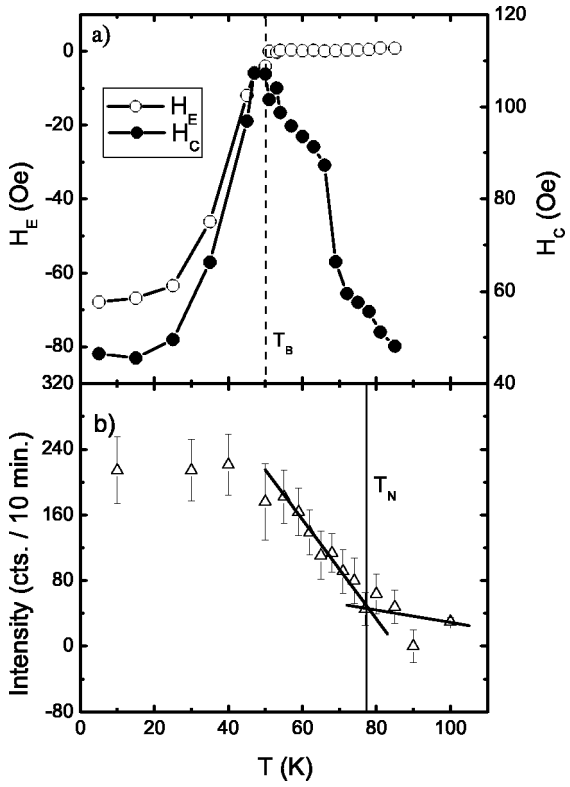

FIG. 11. (a) Exchange bias and coercive field of a 12 nm NiF_2/21.1 nm Co bilayer as a function of temperature after cooling in $H_{CF}=2$ kOe. (b) Temperature dependence of the (001) NiF_2 neutron magnetic integrated peak intensity after field cooling in $H_{CF}=0$. Solid lines are linear fits to the data points close to T_N for $H_{CF}=0$. The intersection of the lines yields T_N. The dashed vertical line indicates T_B and the solid vertical line indicates T_N.

enhancement over the accepted T_N of bulk NiF_2 (73.2 K). The value for the thinnest sample, obtained from Fig. 11, is actually a lower, conservative bound. The actual Néel temperature for this sample could be as high as 85 K, but the relatively weak signal near T_N makes it impossible to obtain a better measurement. An important question is whether T_B is enhanced by a larger T_N of the NiF_2 film. If so, the question is whether it results from a proximity effect, where the Co film, due to its high Curie temperature ($T_C=1388$ K in bulk form), causes the NiF_2 to order at an unusually high temperature. As mentioned above, this has been observed experimentally in Fe_3O_4/CoO multilayers and has also been confirmed theoretically using Monte Carlo simulations.[28] Note that the values of T_N obtained from neutron data with and without field cooling for the 49 nm and 38 nm samples are almost identical, taking into account the error bars, indicating that T_N does not depend on H_{CF}. The background of the magnetic (001) peak is due to the nuclear contribution of the MgF_2 substrate. The integrated intensity of (001) peak (not shown here) gives exactly the same temperature dependence as that of the peak intensity.

We also measured the magnetization along the [110] direction of a 60 nm thick single NiF_2 film with no Co overlayer, in addition to neutron-diffraction measurements. Figure 12(a) shows the NiF_2 (001) peak intensity as a function of temperature after field cooling ($H_{CF}=550$ Oe) and zero-field cooling. Note that $T_N=81$ K, as was the case for the bilayer samples shown in Figs. 9 and 10, indicating that the enhancement of T_N is not due to the proximity effect. Figure 12(b) shows magnetic susceptibility χ, defined as $\chi=M/H$, of this sample with a 2.3 kOe field applied along the NiF_2 [110] direction as a function of temperature, after cooling from $T=100$ K to $T=5$ K in $H_{CF}=2$ kOe. Because NiF_2 is only a weak ferromagnet, the peak in χ corresponds to T_N.[14] The inset of Fig. 12(b) shows $d\chi/dT$, from which we determined that the peak of χ is at $T_N=79.7$ K. This result indeed agrees very well with the neutron-scattering result; the small disagreement may be due to different thermometry set-ups.

TABLE III. Néel (T_N) and blocking (T_B) temperatures for different samples. T_N was determined from neutron diffraction and T_B from magnetization measurements. The 60 nm sample has no Co overlayer and therefore T_B is not available.

NiF_2 thickness (nm)	T_B (K)	T_N (K)
12	53.1±0.5	78(−1+7)
38	81.5±0.5	83.7±2
49	81.0±0.5	82.3±2
60		81.4±2

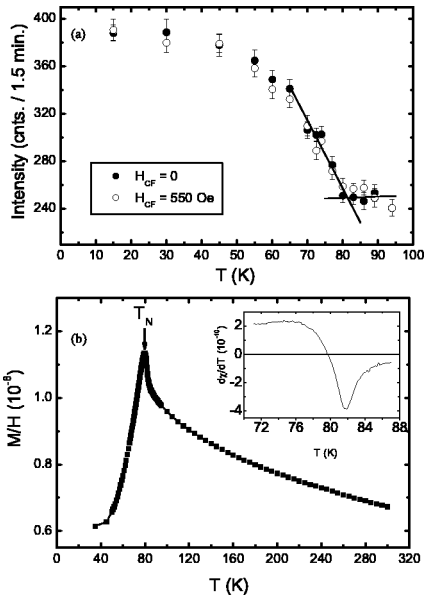

FIG. 12. (a) Temperature-dependent intensity of the (001) magnetic reflection for the 60 nm NiF_2 film after field cooling and zero-field cooling. Note that $T_N=81$ K. Lines are linear fits to the data close to T_N for $H_{CF}=0$. (b) Magnetic susceptibility $\chi=M/H$ as a function of temperature after cooling the sample from $T=100$ K to $T=5$ K in $H_{CF}=2$ kOe. Both the cooling field and the measuring field ($H=2300$ Oe) are parallel to the NiF_2 [110] direction. The inset shows the first derivative of χ with respect to the temperature. $T_N=79.7$ K from the point at which $d\chi/dT=0$.

The values of T_N and T_B for all the samples are shown in Table III.

To interpret the enhancement of the films' T_N with respect to bulk material, we first note that bulk NiF_2 has lattice constants that are similar to those of the MgF_2 substrate. As indicated by the x-ray structural analysis above (Table II), the NiF_2 films grow strained in order to be lattice matched to the substrate crystal structure. This strain causes a significant orthorhombic distortion of the lattice throughout the entire thickness. It is therefore important to determine whether this distortion is responsible for the enhancement of T_N. Unfortunately, the dependence of T_N on pressure or lattice parameters has not been studied in NiF_2, so it is not possible to directly compare our results with experimental data. One may assess this issue by using results from other magnetic materials. Specifically, in many antiferromagnets a change in the unit-cell volume is related to a change in effective exchange interaction by[29]

$$\frac{d(\ln J)}{d(\ln V)} = -\gamma_m, \tag{2}$$

where V is the volume of the unit cell, $d(\ln J)\approx\ln(J_s/J_o)$, and $d(\ln V)\approx\ln(V_s/V_o)$. Here J_s and V_s refer to the sample exchange and volume, respectively, and J_o and V_o refer to the exchange and volume of the bulk crystal. This γ_m is an effective magnetic Grüneisen constant which for a wide array of magnetic materials $\gamma_m=10/3$, including FeF_2 (Ref. 30) and MnF_2.[31] Assuming that NiF_2 obeys the 10/3 law; using the mean-field result that $T_N\propto J$ (known to be accurate for calculating changes in T_N) (Ref. 32); and using $V=2d_{110}d_{110}d_{001}$, we obtain that $\Delta T_N=2.4$ K. This is smaller than our experimental value of ≈ 8 K by a factor of 3. The lattice mismatch at low temperatures between MgF_2 and NiF_2 is smaller than at room temperature,[33] so the expected change in T_N discussed here is an upper bound. The large relative change of the *c*-axis lattice parameter would seem to indicate that a change in J_1 might be responsible for the enhanced T_N, but this is unlikely because J_1 is more than 60 times smaller in magnitude than J_2.

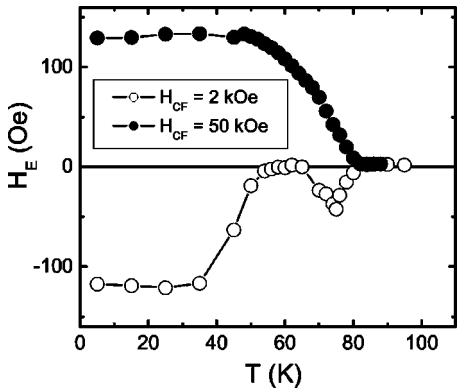

FIG. 13. Exchange bias for two cooling fields as a function of temperature for the 38 nm NiF_2/15.9 nm Co sample.

Our results therefore suggest that γ_m is anomalous for NiF_2. One possibility is that the fluorine ions are displaced from their equilibrium positions, independent of the lattice expansion or contraction, which could have a significant effect on the exchange interactions. NiF_2 is known to have a significant magnetostrictive shift of the fluorine ions at low T with respect to the value above T_N, unlike FeF_2.[33,34] Further neutron and x-ray measurements are needed todetermine whether this is the case.

D. Reentrant exchange bias

Figure 10 shows the exchange bias and the NiF_2 (001) peak intensity as a function of temperature in the 38 nm bilayer sample. For a small cooling field ($H_{CF}=2$ kOe) H_E shows a reentrant behavior. In other words, it goes to zero at $T\sim 55$ K and then becomes negative before it vanishes again at $T=81$ K. On the other hand, if the cooling field is sufficiently large ($H_{CF}=50$ kOe, see Fig. 13), H_E remains positive before it vanishes at the same blocking temperature, $T_B=81$ K. This behavior is similar to the change in sign of H_E as a function of T in $Fe_xZn_{1-x}F_2$/Co bilayers, with $x\sim 0.80$, where H_E can be zero at an intermediate temperature for moderate cooling fields.[35] For the case of the NiF_2, when H_E goes to zero as the sample is warmed, instead of becoming positive at higher temperatures, it becomes negative once again. It is unclear whether the change in sign of H_E in $Fe_xZn_{1-x}F_2$ and the reentrant effect in NiF_2 are related. However, it is possible that for NiF_2 this is a result of a reorientation of the antiferromagnetic domains from the (100) plane to the (010) plane or vice versa. A similar reentrant effect, although less marked, has been observed in $FePt_3$/Fe

bilayers[36] and its origin is believed to result from a spin reorientation in the antiferromagnet, similar to the one discussed here, that has been observed via neutron scattering.[37] Further neutron-diffraction measurements of the magnetic (100) peak are planned to determine whether this is true. Unfortunately a substrate contamination peak precluded us from performing these measurements with high accuracy in these samples, so better substrates will be needed.

E. Reduction of T_B in thin NiF_2

Figure 11(a) shows H_E as a function of temperature for a 12 nm thick NiF_2 sample. In this case T_B is reduced to $T \approx 53$ K. However, the integrated NiF_2 (001) peak intensity, as shown in Fig. 11(b), indicates that $T_N \approx 78$ K, with an uncertainty of approximately $-1+7$ K. Hence, T_N is certainly above 70 K, and is possible as high as 85 K. Note that all the data in Fig. 11(b) are plotted after subtracting the nuclear MgF_2 (001) peak measured at $T=90$ K. This shows that the reduced T_B is not due to a diminished T_N, but is probably due to the AF domains in the NiF_2 becoming unpinned above $T=53$ K. This is consistent with measurements in single crystals that suggest that the magnetization in the *a-b* plane becomes isotropic close to T_N.[14] It is not surprising that for small NiF_2 thicknesses this effect would be magnified because the total magnetic anisotropy energy is proportional to the volume, and therefore, the thickness of the film. It is also interesting to note that the temperature at which H_E goes to zero for the first time (53 K) in the 38 nm sample coincides with T_B for the 12 nm sample. Further measurements are required to determine whether this is a coincidence, or if $T=50$ K is the temperature where the magnetic in-plane anisotropy of the NiF_2 "softens" up. In any case, this is a clear experimental demonstration that, in general, a low T_B is not necessarily due to a lower T_N, due to finite-size effects, for example, but could be due to other factors, such as a smaller effective anisotropy energy that can no longer withstand its magnetic structure at higher temperatures.

IV. CONCLUSIONS

In summary, (110) NiF_2 was epitaxially grown on (110) MgF_2 substrates via MBE. In thicker NiF_2, T_N and T_B are significantly larger than the bulk value. This enhancement of T_N is likely to be a result of the strain in NiF_2 due to a small lattice mismatch between the NiF_2 films and the MgF_2 substrates. In order to calculate the enhancement of T_N due to the strain in NiF_2, the dependence of J_2 not only on the lattice parameters, but possibly also on the position of the fluorine ions is needed. A reentrant exchange bias behavior was also observed for the 38 nm sample. For the thinnest, 12 nm sample, $T_B \ll T_N$, indicating that the antiferromagnet's anisotropy is not enough to maintain the exchange bias at higher temperatures below T_N, even though long-range order in NiF_2 is maintained.

ACKNOWLEDGMENTS

This work was supported in part by the National Science Foundation (Grant No. EPS-0083046) at WVU.

*Present address: Department of Physics, University of California, Irvine, CA 92697-4560.

[1] W. H. Meiklejohn and C. P. Bean, Phys. Rev. **102**, 1413 (1956).
[2] J. Nogués and I. K. Schuller, J. Magn. Magn. Mater. **192**, 203 (1999).
[3] A. E. Berkowitz and K. Takano, J. Magn. Magn. Mater. **200**, 552 (1999).
[4] S. Soeya, S. Nakamura, T. Imgawa, and S. Narishige, J. Appl. Phys. **77**, 5838 (1995).
[5] M. S. Lund, W. A. A. Macedo, K. Liu, J. Nogués, I. K. Schuller, and C. Leighton, Phys. Rev. B **66**, 054422 (2002).
[6] S. S. P. Parkin and V. S. Speriosu, in *Magnetic Properties of Low-Dimensional Systems II. New Developments*, Proceedings of the Second Workshop, edited by L. M. Falicov, F. Mejía Lira, and J. L. Morán-López (Springer-Verlag, Berlin, 1990), p. 110.
[7] D. Lederman, C. A. Ramos, V. Jaccarino, and J. L. Cardy, Phys. Rev. B **48**, 8365 (1993).
[8] P. J. van der Zaag, Y. Ijiri, J. A. Borchers, L. F. Feiner, R. M. Wolf, J. M. Gaines, R. W. Erwin, and M. A. Verheijen, Phys. Rev. Lett. **84**, 6102 (2000).
[9] H. Yamazaki and J. Satooka, J. Magn. Magn. Mater. **240**, 442 (2002).
[10] J. W. Stout and S. A. Reed, J. Am. Chem. Soc. **76**, 5279 (1954).
[11] T. Moriya, Phys. Rev. **117**, 635 (1960).
[12] M. T. Hutchings, M. F. Thorpe, R. J. Birgeneau, P. A. Fleury, and H. J. Guggenheim, Phys. Rev. B **2**, 1362 (1970).
[13] J. W. Stout and E. Catalano, J. Chem. Phys. **23**, 1284 (1955).
[14] A. S. Borovik-Romanov, A. N. Bazhan, and N. M. Kreines, Zh. Eksp. Teor. Fiz. **64**, 1367 (1973) [Sov. Phys. JETP **37**, 695 (1973)].
[15] A. S. Pavlovic, Phys. Rev. B **21**, 3652 (1980).
[16] J. Nogués, T. J. Moran, D. Lederman, I. K. Schuller, and K. V. Rao, Phys. Rev. B **59**, 6984 (1999).
[17] J. McChesney, M. Hetzer, H. Shi, T. Charlton, and D. Lederman, J. Mater. Res. **16**, 1769 (2001).
[18] B. Vidal and P. Vincent, Appl. Opt. **23**, 1794 (1984).
[19] T. C. Schulthess and W. H. Butler, Phys. Rev. Lett. **81**, 4516 (1998).
[20] R. A. Erickson, Phys. Rev. **90**, 779 (1953).
[21] H. Shi and D. Lederman, Phys. Rev. B **66**, 094426 (2002).
[22] W. Baur, Acta Crystallogr., Sect. B: Struct. Crystallogr. Cryst. Chem. **B32**, 2200 (1976).
[23] C. Leighton, H. Suhl, M. J. Pechan, R. Compton, J. Nogués, and I. K. Schuller, J. Appl. Phys. **92**, 1483 (2002).
[24] H. Shi, D. Lederman, and E. E. Fullerton, J. Appl. Phys. **91**, 7763 (2002).
[25] M. Grimsditch, A. Hoffmann, P. Vavassori, H. Shi, and D. Lederman, Phys. Rev. Lett. **90**, 257201 (2003).
[26] I. N. Krivorotov, C. Leighton, J. Nogués, I. K. Schuller, and E. D. Dahlberg, Phys. Rev. B **68**, 054430 (2003).

[27] J. Nogués, D. Lederman, T. J. Moran, and I. K. Schuller, Phys. Rev. Lett. **76**, 4624 (1996).
[28] S. H. Tsai, D. P. Landau, and T. C. Schulthess, J. Appl. Phys. **93**, 8612 (2003).
[29] D. Bloch, J. Phys. Chem. Solids **27**, 881 (1966).
[30] G. A. Garcia and R. Ingalls, J. Phys. Chem. Solids **37**, 211 (1975).
[31] K. C. Johnson and A. J. Sievers, Phys. Rev. B **10**, 1027 (1974).
[32] G. K. Wertheim, H. J. Guggenheim, M. Butler, and V. Jaccarino, Phys. Rev. **178**, 804 (1969).
[33] W. Jauch, Phys. Rev. B **44**, 6864 (1991).
[34] A. Palmer and W. Jauch, Phys. Rev. B **48**, 10 304 (1993).
[35] H. Shi, D. Lederman, N. R. Dilley, R. C. Black, J. Diedrichs, K. Jensen, and M. B. Simmonds, J. Appl. Phys. **93**, 8600 (2003).
[36] R. L. Compton, M. J. Pechan, S. Maat, and E. E. Fullerton, Phys. Rev. B **66**, 054411 (2002).
[37] S. Maat, O. Hellwig, G. Zeltzer, E. E. Fullerton, G. J. Mankey, M. L. Crow, and J. L. Robertson, Phys. Rev. B **63**, 134426 (2001).